

**Pressure-induced phase transition in pyrochlore iridates $(\text{Sm}_{1-x}\text{Bi}_x)_2\text{Ir}_2\text{O}_7$
($x = 0, 0.02, \text{ and } 0.10$): Raman and X-ray diffraction studies**

M Rosalin,¹ K.A. Irshad,² Bobby Joseph,² Prachi Telang,³
Surjeet Singh,³ D V S Muthu,¹ and A K Sood^{1,*}

¹*Department of Physics, Indian Institute of Science, Bangalore, 560012, India*

²*Elettra-Sincrotrone Trieste S.C. p.A., S.S. 14,
Km 163.5 in Area Science Park, Basovizza 34149, Italy*

³*Department of Physics, Indian Institute of Science
Education and Research, Pune, Maharashtra, 411008, India*

Abstract

The pyrochlore iridates, $A_2\text{Ir}_2\text{O}_7$, show a wide variety of structural, electronic, and magnetic properties controlled by the interplay of different exchange interactions, which can be tuned by external pressure. In this work, we report pressure-induced phase transitions at ambient temperature using synchrotron-based X-ray diffraction (up to ~ 20 GPa) and Raman-scattering measurements (up to ~ 25 GPa) of the pyrochlore series $(\text{Sm}_{1-x}\text{Bi}_x)_2\text{Ir}_2\text{O}_7$ ($x = 0, 0.02, \text{ and } 0.10$). Our Raman and X-ray data suggest an iso-structural transition in $\text{Sm}_2\text{Ir}_2\text{O}_7$ at $P_c \sim 11.2$ GPa associated with the rearrangement of IrO_6 octahedra in the pyrochlore lattice. The transition pressure decreases to ~ 10.2 and 9 GPa for $x = 0.02$ and 0.10 , respectively. For all the samples, the linewidth of three phonons associated with Ir-O-Ir (A_{1g} and E_g) and Ir-O (T_{2g}^4) vibrations show anomalous decrease up to P_c , due to decrease in electron-phonon interaction.

I. INTRODUCTION

Pyrochlore iridates have emerged as an interesting family of materials, providing a unique framework for studying the interplay of electronic correlations, spin-orbit coupling, and topological phenomena. These compounds, $A_2\text{Ir}_2\text{O}_7$, where A is a rare earth element, have drawn particular interest due to their intricate electronic and magnetic behavior that sets the stage for the exploration of novel quantum phenomena and topological phases [1–5]. By substituting the A site successively with larger rare-earth atoms, the physical properties evolve with the A -site cation radius from magnetic insulating to a complex nonmagnetic metallic behavior [6–10]. In the lanthanide series, from Lu to Gd, iridates show insulating behavior; Eu, Sm, and Nd iridates show a metal-insulator transition (MIT) with the transition temperature varying as a function of rare earth ionic radius [9, 11, 12]. However, the end member $\text{Pr}_2\text{Ir}_2\text{O}_7$ remains metallic even at low temperatures [10]. Increasing A size in the $A_2\text{Ir}_2\text{O}_7$ series results in a broader Ir-O-Ir bond angle and shorter Ir-O bond lengths. As a result, the iridium t_{2g} bandwidth widens and eventually surpasses the metallization threshold at a given A ionic radius [12].

Application of chemical pressure i.e., doping A^{3+} or Ir^{4+} sites, and physical pressure, have proven effective tools to tune the relative scale of interactions and electronic bandwidth in this class of materials. Expanding the size of the A cation results in a simultaneous increase in the Ir-O-Ir bond angle and lattice parameter [12]. In contrast, under hydrostatic pressure, the Ir-O-Ir

* asood@iisc.ac.in

bond angle increases while the lattice parameter decreases [13]. Hence it would be interesting to explore whether the bandwidth can be tuned by applying a combination of chemical and hydrostatic pressures in a systematic manner.

Recently, it has been reported that $\text{Sm}_2\text{Ir}_2\text{O}_7$ doped with Bi (lattice constant $a = 10.3235 \text{ \AA}$ for $\text{Sm}_2\text{Ir}_2\text{O}_7$ and 10.3250 \AA for $\text{Bi}_2\text{Ir}_2\text{O}_7$) shows anomalous lattice contraction up to 10 % Bi doping, followed by normal lattice expansion with further Bi substitution [14]. This series of iridates provides an interesting system to see the effect of the hydrostatic pressure with systematic chemical substitution. Both Raman spectroscopy and X-ray diffraction (XRD) are powerful tools for characterizing the structural changes induced by pressure. Raman spectroscopy enables the investigation of vibrational modes, providing information about local atomic environments and structural distortions, while XRD provides information on crystallographic changes. The synergy between these techniques allows for a comprehensive analysis of the material’s response to pressure.

In this study, we systematically investigate the $(\text{Sm}_{1-x}\text{Bi}_x)_2\text{Ir}_2\text{O}_7$ (SBIO) series for $x = 0, 0.02,$ and 0.10 to explore the influence of chemical tuning on the high-pressure behavior of these compounds. Our goal is to unravel how the delicate balance between electron-lattice interactions and chemical composition governs the observed structural transformations. An iso-structural transition in $\text{Sm}_2\text{Ir}_2\text{O}_7$ at $\sim 11.2 \text{ GPa}$, marked P_c , is suggested by our Raman and X-ray data, which is linked to the rearrangement of IrO_6 octahedra in the pyrochlore lattice. The linewidths of the Ir-O-Ir bending (A_{1g} and E_g) and Ir-O stretching (T_{2g}^4) vibrations exhibit anomalous drop with pressure up to P_c for all the three samples. This decrease is caused by a decrease in the electron-phonon interaction due to the increased electronic bandwidth of these materials with pressure. The critical pressure P_c decreases to ~ 10.2 and 9 GPa for $x = 0.02$ and 0.10 , respectively.

II. EXPERIMENTAL DETAILS

All the samples in the SBIO series ($x = 0, 0.02,$ and 0.10) were synthesized via solid-state reaction method using high purity (99.9 %) precursors of Sm_2O_3 , IrO_2 , and Bi_2O_3 . The details of sample synthesis and characterization are given in [14, 15]. The high-pressure XRD measurements were carried out at Xpress beamline, Elettra, in Italy, using a monochromatic XRD wavelength (λ) of 0.4957 \AA at room temperature. Standard CeO_2 powder sample was used for calibrating the sample-to-detector distance and orientation angles of the detector. The SBIO pel-

lets ($x = 0, 0.02, \text{ and } 0.10$) were finely ground and put into membrane-type diamond-anvil cells (DACs) with a culet diameter of $\sim 400 \mu\text{m}$ for the XRD measurements. The pressure-transmitting medium (PTM) used for the membrane-type DAC was methanol: ethanol solution (4:1); and the applied pressure was measured using a ruby fluorescence marker [16–18]. Two-dimensional (2D) diffraction patterns were captured using a Dectris Pilatus 6M detector, and subsequently, these patterns were transformed into $I(2\theta)$ diffraction profiles by radial integration of the diffraction rings using FIT2D software [19]. The structural analysis involved fitting and refining the raw data using a conventional Rietveld refinement procedure, facilitated by the GSAS software package [20]. High-pressure Raman scattering experiments at room temperature were carried out in backscattering geometry using a 50X objective in a Horiba LabRAM HR Evolution Spectrometer equipped with a DPSS laser source of wavelength 532 nm and $\sim 1.5 \text{ mW}$ of laser power on the sample. The DAC used for Raman measurements was Mao-Bell type with two 16-facet brilliant cut diamonds with culet diameter size of $\sim 600 \mu\text{m}$. The experiments were carried out on a small piece ($\sim 75 \mu\text{m}$) taken from polycrystalline sintered pellets of Bi-doped $\text{Sm}_2\text{Ir}_2\text{O}_7$ samples. The sample was placed inside a stainless-steel gasket hole with a diameter of $\sim 150 \mu\text{m}$. For doped $\text{Sm}_2\text{Ir}_2\text{O}_7$, the pressure was applied using a 4:1 methanol-ethanol combination as PTM that had a freezing pressure of $\sim 10.4 \text{ GPa}$ [21]. However, for $\text{Sm}_2\text{Ir}_2\text{O}_7$, liquid distilled H_2O was used as the PTM as the methanol-ethanol solution was giving rise to a large background and poor signal-to-noise ratio. The spectra were acquired using a thermoelectrically cooled charge-coupled device (CCD) (HORIBA Jobin Yvon, SYNCERITY 1024 \times 256). The recorded Raman spectra are fitted with a sum of Lorentzian line shapes using the nonlinear least square fitting method in the Origin software package [22] to extract phonon frequencies, linewidths, and intensities.

III. RESULTS AND DISCUSSIONS

A. High-pressure XRD studies

The structural stability of SBIO under pressure was investigated at room temperature up to $\sim 20.4, 19.6, \text{ and } 20.3 \text{ GPa}$ for samples with $x = 0, 0.02, \text{ and } 0.10$, respectively. The angle dispersive powder XRD patterns of SBIO at various high pressures at 300 K are shown in Fig. 1 (a-c). These diffraction patterns show that all of the Bragg peaks shift in the direction of increasing 2θ angles as pressure increases, inferring the expected gradual contraction of the lattice. Further,

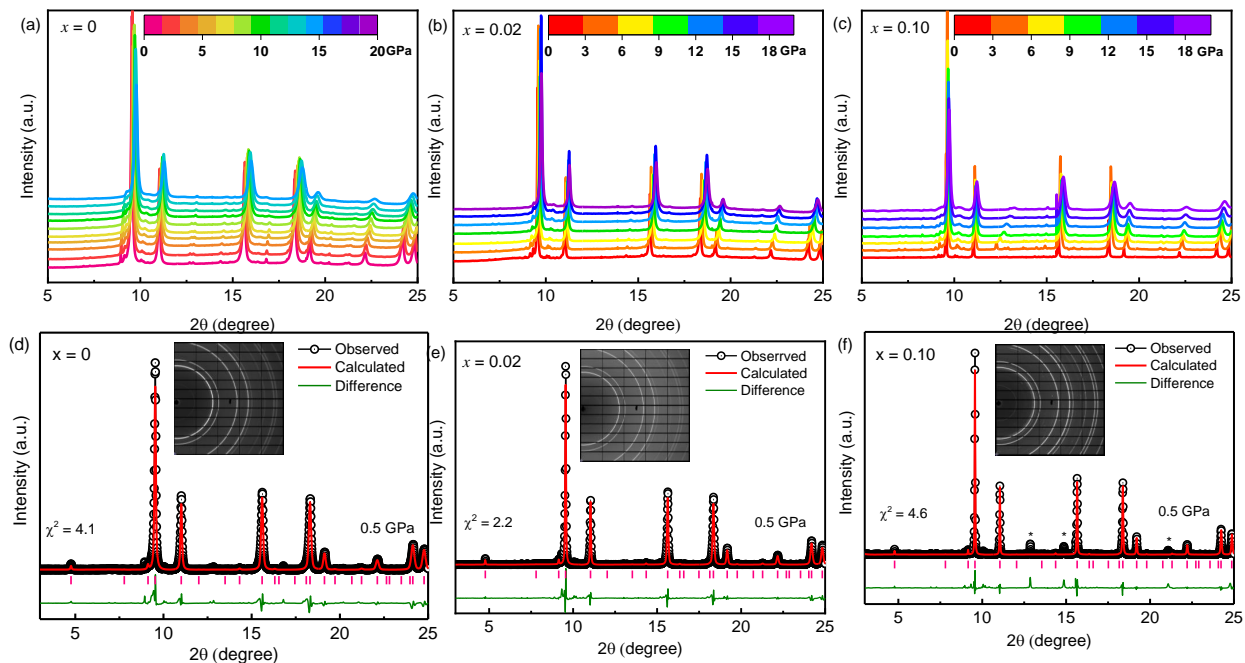


FIG. 1. (a-c) Angle dispersive X-ray diffraction patterns of $(\text{Sm}_{1-x}\text{Bi}_x)_2\text{Ir}_2\text{O}_7$ (SBIO) series for $x = 0, 0.02,$ and $0.10,$ respectively at selected pressures ranging from 0.2 to 20 GPa. (d-f) Rietveld refined XRD patterns at 0.5 GPa with the Debye-Scherrer ring pattern shown in the insets. Solid circles indicate experimental data and the star symbols in the (f) panel mark the Ir metal impurity peaks. Calculated patterns are drawn as red solid lines. Bragg reflection positions are indicated by vertical bars. Lower dark green curves are the difference between the observed and calculated profiles.

the diffraction peaks significantly broaden at higher pressures due to strain-broadening. However, the absence of any new Bragg peak or of existing peaks splitting indicates absence of structural phase transition under pressure. Figure 1 (d-f) shows the Rietveld fitted diffraction profiles for ambient pressure cubic pyrochlore phase having space group $\text{Fd}\bar{3}\text{m}$ ($z = 8$). The lattice parameters, atomic positions, line shape, and background were all refined in this process and the goodness-of-fit parameter (χ^2) given in Fig. 1 indicates that the quality of the refinements remains good throughout the SBIO series. In Fig. 2 (a-c), the volume of the unit cell (estimated using the lattice parameter value from Rietveld refinement of SBIO series) is plotted against pressure which shows the cubic lattice volume decreases with increasing pressure. The P - V data are fitted by a third-order Birch-Murnaghan (BM) equation of state (EOS) [23] given by,

$$P = \frac{3B}{2} \left[\left(\frac{V_0}{V} \right)^{\frac{7}{3}} - \left(\frac{V_0}{V} \right)^{\frac{5}{3}} \right] \times \left\{ \left[1 + \frac{3}{4} (B' - 4) \right] \left[\left(\frac{V_0}{V} \right)^{\frac{2}{3}} \right] \right\} \quad (1)$$

where B represents the bulk modulus or the modulus of incompressibility at ambient pressure, B' represents the first derivative of the bulk modulus with respect to pressure, and V_0 represents the unit cell volume at ambient pressure. The extracted values from the fit are $B = 198.4 \pm 4.0$ GPa and $B' = 7.8 \pm 0.8$ for $x = 0$, which compares well with the previously reported value for $\text{Eu}_2\text{Ir}_2\text{O}_7$ [24, 25] and recent preprint on $\text{Sm}_2\text{Ir}_2\text{O}_7$ [26]. The fit parameters for doped samples are, $B = 214.7 \pm 6.3$ GPa and $B' = 8.5 \pm 2.4$ for $x = 0.02$, and $B = 250.5 \pm 9.6$ GPa and $B' = 18.5 \pm 4.0$ GPa for $x = 0.10$. The value of B' becomes noticeably large in the case of $x = 0.10$, indicating that doped SBIO ($x = 0.10$) stiffens rapidly under pressure. It is clear from Fig. 2 that the P - V plot for all the samples can be fitted over the entire pressure window upto ~ 20 GPa. However, the signatures of a transition at P_c , not reported so far, are clearly seen in the pressure dependence of the unit cell parameters derived from the Rietveld refinement plotted in Fig. 2 (d-o). In the pyrochlore structure, each Ir-site cation is coordinated to six O (48f) ions, forming an IrO_6 octahedron which has a variable u -coordinate, the only free parameter in the pyrochlore structure besides the lattice parameter, a . The perfect octahedral symmetry is achieved for $u = 0.3125$. The pyrochlore stability field lies within the interval of $0.3125 \leq u \leq 0.375$, and the IrO_6 octahedral exhibits a trigonal compression that increases with u [24, 27, 28]. The evolution of u as a function of pressure in Fig. 2 (d) shows a finite increase with a jump near P_c , suggesting that the IrO_6 octahedra become increasingly more distorted at higher pressures with a sudden change in the degree of distortion occurring at P_c , likely due to an iso-structural transition implying a rearrangement of the IrO_6 octahedra. The increase in u in $\text{Sm}_2\text{Ir}_2\text{O}_7$ with pressure is similar to $\text{Eu}_2\text{Ir}_2\text{O}_7$ [24], but in the recent high-pressure preprint on $A_2\text{Ir}_2\text{O}_7$ ($A = \text{Pr}, \text{Sm}, \text{Dy-Lu}$), u remains constant over increasing pressure [26]. Since the pressure-dependent XRD patterns do not reveal any new diffraction peak or splitting of lines, it is inferred that the structural deformation at $\sim P_c$ is a local distortion. It is possible that as the pressure increases, due to vacancies at the 8a sites, the Ir^{4+} ions adjust their local coordinates, causing other atoms in the lattice to relocate, retaining the cubic symmetry and affecting oxygen positions (u) in the IrO_6 octahedra as reflected in the abrupt change in u near at P_c [29]. The corresponding Ir-O-Ir bond angle (Fig. 2 (g)) and Ir-O bond

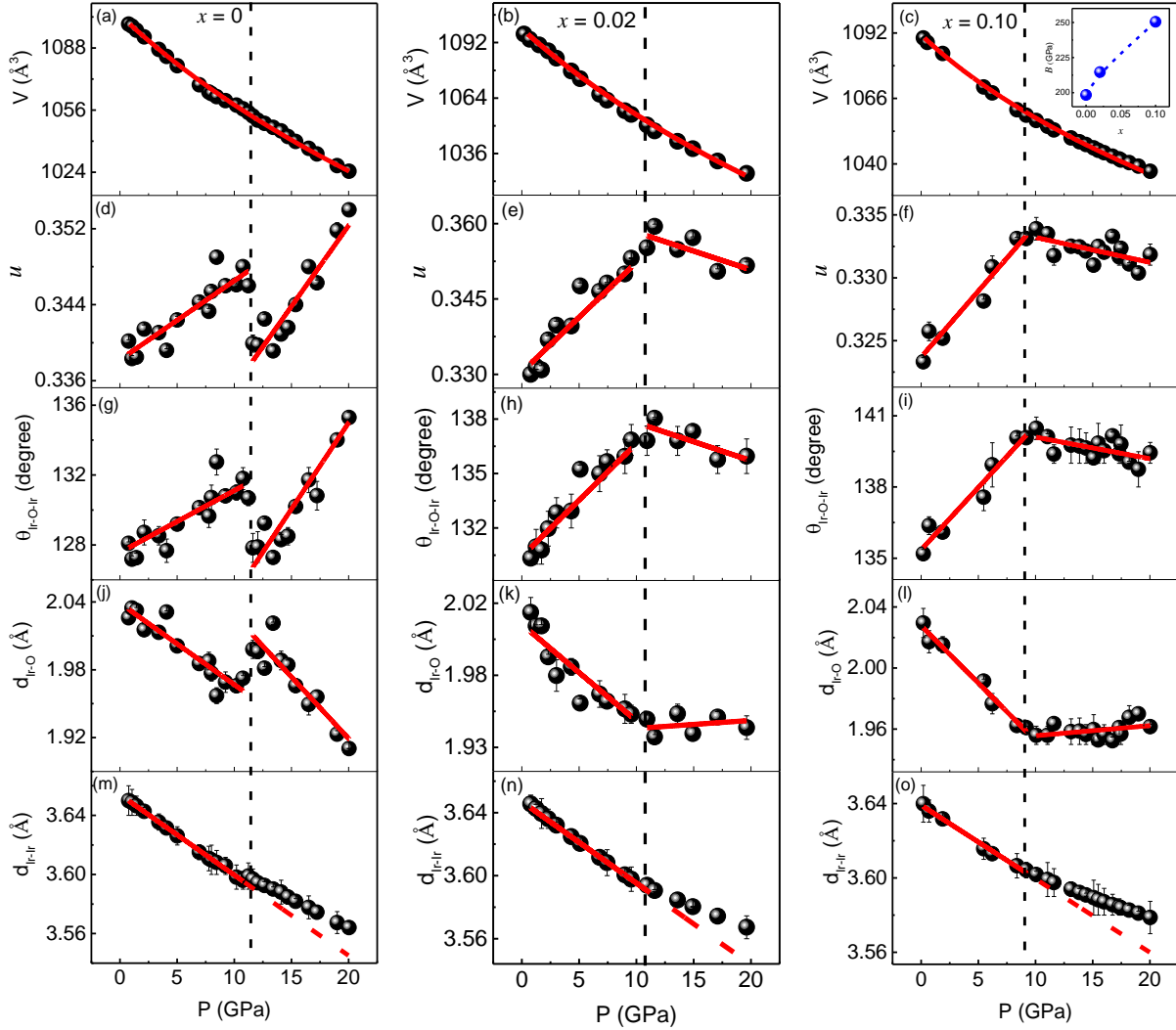


FIG. 2. (a-c) Pressure dependence of lattice volume in the pyrochlore phase of SBIO ($x = 0, 0.02,$ and $0.10,$ respectively), fitted (solid red line) P - V diagram using a third-order Birch–Murnaghan equation of state. Inset in the rightmost top panel show the variation of the bulk modulus (B) with doping concentration x .(d-o) The pressure dependence of the Rietveld refinement parameters, Oxygen coordinate (u), Ir-O-Ir bond angle ($\theta_{Ir-O-Ir}$), Ir-Ir (d_{Ir-Ir}), and Ir-O bond distance (d_{Ir-O}), respectively for SBIO ($x = 0, 0.02,$ and 0.10). The vertical dashed lines in each panel indicate P_c and the linear fit below P_c is extrapolated above P_c by dashed red lines in panels m,n, and o.

length (Fig. 2 (j)) also show discontinuities near P_c . The pressure coefficient of Ir-Ir bond length (Fig. 2 (m)) also shows a clear change at P_c . The inset of Fig. 2 (c) shows the increase of the bulk modulus with the doping concentration x . Increasing values of bulk modulus with increasing x is

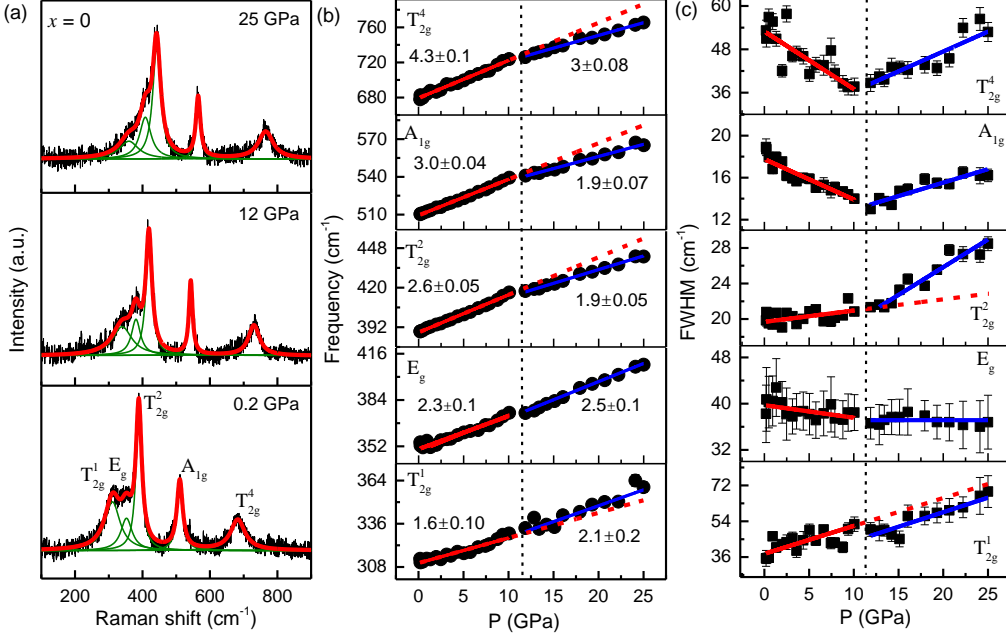


FIG. 3. (a) Fitted Raman spectra of $\text{Sm}_2\text{Ir}_2\text{O}_7$ at some representative pressures. Dark green curves are individual fit to the phonon modes, and solid red curves are cumulative fit to the spectra. (b-c) The pressure dependence of frequencies and linewidths, respectively, of various phonon modes up to 25 GPa. Solid red and blue lines are linear fit to the data below and above P_c , respectively. The vertical dashed lines indicate P_c and the linear fit below P_c is extrapolated above P_c by dashed red lines in (b) and (c).

expected, following the anomalous lattice contraction in SBIO from $x = 0$ to 0.10. It may be noted that all the four lattice characteristics for $x = 0.02$ and 0.10 samples also change at $P \sim 10.2$ and 9 GPa, respectively in Fig. 2 (e-f, h-i, k-l, n-o). The decrease in P_c with x can be attributed to the anomalous lattice contraction in SBIO.

B. High-pressure Raman studies on $\text{Sm}_2\text{Ir}_2\text{O}_7$

Based on group theory, the pyrochlore structure (space group $\text{Fd}\bar{3}\text{m}$) has zone-center optical, $\Gamma_{op} = A_{1g} + E_g + 4T_{2g} + 7T_{1u}$ and acoustic, $\Gamma_{ac} = T_{1u}$ phonon modes [30]. The Raman active phonons are A_{1g} , E_g , and $4T_{2g}$, and the rest seven are IR active. The Raman modes are assigned with irreducible representations, as shown in Fig. 3 (a), based on prior reports on pyrochlore iridates [30, 31]. The mode assignments are as follows: A_{1g} and E_g modes involve Ir-O-Ir bending, T_{2g}^1 and T_{2g}^2 modes associated with Sm-O stretching, T_{2g}^3 mode due to the vibration of O' ions surrounded by eight Sm ions and T_{2g}^4 mode related to Ir-O stretching vibration [30]. As

the cation sites of Ir^{4+} and Sm^{3+} have center of inversion, the Raman active modes involve only the vibrations of oxygen atoms. Figure S1 shows the pressure evolution of the Raman modes at some representative pressures. Raman spectrum at the lowest pressure inside the DAC for $\text{Sm}_2\text{Ir}_2\text{O}_7$ is plotted in the bottommost panel of Fig. 3 (a), which shows five phonon modes. The position and relative intensities of these bands agree well with the literature [30, 31]. T_{2g}^3 is a weak mode and could not be detected inside the DAC. Raman spectra at an intermediate and highest pressure are shown in the middle and topmost panel in Fig. 3 (a). The same number of phonon modes are observed with varying pressure which confirms the preservation of crystal symmetry with pressure, in agreement with the XRD results. The individual phonon modes were fitted with Lorentzian line shape as shown in Fig. 3 (a), and the extracted phonon frequencies and linewidths are plotted against pressure in Figs. 3 (b) and (c). The straight lines represent the fitting of mode frequencies using the linear equation, $\omega_P = \omega_0 + \left(\frac{d\omega}{dP}\right) P$, where ω_0 is the mode frequency at ambient pressure. All the phonon modes demonstrate expected hardening with increasing pressure due to the compression of the unit cell, resulting in an increase in the stiffness constant (K) associated with the vibrational mode. However, we observe an alteration of the pressure-coefficients ($d\omega/dP$) of the phonon mode frequencies across $P_c \sim 11.2$ GPa, supporting the presence of an iso-structural transition as inferred by the XRD results. It should be noted that we have performed the high-pressure experiment with distilled water as the PTM, which starts freezing above 1 GPa, making it a quasi-hydrostatic pressure medium. Therefore, the anomalies near P_c are unlikely to be triggered by the non-hydrostatic nature of the medium. Further, our XRD data using methanol: ethanol as PTM also exhibit anomalies near P_c , indicating that the transition is intrinsic to the system. A previous high-pressure study on $\text{Gd}_2\text{Ti}_2\text{O}_7$ has also shown that the pressure dependence of the Raman modes is seen to be similar in both methanol-ethanol mixture and distilled water as PTM [32]. The two high-pressure iso-structural phases are associated with a positive slope value for all the phonon modes, as depicted in Fig. 3 (b). To quantify the phonon frequency changes under pressure we have estimated the Grüneisen parameter (γ) given by,

$$\gamma = \frac{B}{\omega_0} \frac{d\omega}{dP} \quad (2)$$

below and above P_c for all the phonon modes. The values are listed in Table I. The significant changes in γ suggest a subtle structural deformation, as seen in pressure-dependent XRD measurements (see Fig. 2).

To understand the frequency variations in $\text{Sm}_2\text{Ir}_2\text{O}_7$, we compared the effect of physical and

Modes	$P < P_c$	$P > P_c$
T_{2g}^1	1.04	1.35
E_g	1.28	1.42
T_{2g}^2	1.35	0.95
A_{1g}	1.12	0.72
T_{2g}^4	1.25	0.85

TABLE I. Grüneisen parameter (γ) for various phonon modes below and above P_c for $x = 0$

chemical pressure, similar to our earlier high-pressure work on $\text{Eu}_2\text{Ir}_2\text{O}_7$ [30]. As an effect of A -site cation radius, the lattice volume decreases by $\sim 32 \text{ \AA}^3$, coming from $\text{Pr}_2\text{Ir}_2\text{O}_7$ to $\text{Sm}_2\text{Ir}_2\text{O}_7$ in the pyrochlore series [33]. The difference in phonon frequencies for the A_{1g} mode in $\text{Sm}_2\text{Ir}_2\text{O}_7$ compared to $\text{Pr}_2\text{Ir}_2\text{O}_7$ is $\sim 2 \text{ cm}^{-1}$ [30]. Our P - V data (Fig. 2 (a)) indicates that a volume reduction of 32 \AA^3 equates to a pressure of $\sim 7 \text{ GPa}$, causing the A_{1g} mode frequency to harden by $\sim 18 \text{ cm}^{-1}$. The significant difference in frequency shifts for the A_{1g} phonon due to physical and chemical pressures cannot be explained only by the quasiharmonic effect, indicating that the A_{1g} phonon is also renormalized by an underlying electron-phonon interaction. It can be seen from Fig. 2 that the Ir-Ir and Ir-O bond distances systematically decrease up to P_c , and thus increasing electronic bandwidth in a metal by enhancing the hybridization of the Ir- $5d$ and O- $2p$ orbitals, and direct hopping between the Ir sites [12, 13]. Similarly, an increase in the Ir-O-Ir bond angle would favor electrons hopping between two Ir atoms via the oxygen atom and contribute to the increasing bandwidth. Thus, the large frequency variation of the A_{1g} mode in $\text{Sm}_2\text{Ir}_2\text{O}_7$ can be correlated with the increase in the electronic bandwidth leading to significant changes in the electron-phonon interaction [34].

Figure 3 (c) depicts the pressure evolution of linewidths for the five strongest Raman phonons, showing an unexpected drop in the linewidth of the Ir-O-Ir bending (A_{1g} and E_g) as well as Ir-O stretching vibrations T_{2g}^4 upto P_c . The solid lines are linear fit to $\Gamma = \Gamma_0 + \left(\frac{d\Gamma}{dP}\right) P$. It can be seen that $\frac{d\Gamma}{dP}$ is negative for A_{1g} , E_g , and T_{2g}^4 modes. The values of $\frac{d\Gamma}{dP}$ are given in table II. This observation is similar to our recent high-pressure Raman study on $\text{Eu}_2\text{Ir}_2\text{O}_7$, where an equivalent linewidth drop was seen for the A_{1g} phonon [25]. One possible explanation for the anomalous decrease in the linewidth of these modes is a decrease in the electron-phonon interaction due to pressure. Since this anomaly is observed in phonons related to Ir-O and Ir-O-Ir vibrations, it can

be correlated with the observed systematic trend of the Ir–Ir and Ir–O bond distance as well as the Ir–O–Ir bond angle up to P_c which increases the electronic bandwidth, thereby decreasing the electron-phonon interaction. According to the Holstein model, the electronic-phonon interaction strength in a metal, $\lambda = 2g^2/W\omega$ (where ω is the phonon frequency, t is the nearest-neighbor hopping integral, $W = 8t$ is the electronic bandwidth, and g is the coupling constant), will vary inversely with its electronic bandwidth [35]. As seen in Fig. 2, $\theta_{Ir-O-Ir}$ increases with pressure, increasing the electronic bandwidth and thus decreasing λ and the observed linewidth drop. The linewidth of other T_{2g}^1 and T_{2g}^2 phonons increases with increasing pressure which can be attributed to the corresponding change in the two-phonon density of states, which affects the anharmonic interactions [36].

Modes	$x = 0$		$x = 0.02$		$x = 0.10$	
	$P < P_c$	$P > P_c$	$P < P_c$	$P > P_c$	$P < P_c$	$P > P_c$
T_{2g}^1	1.4 ± 0.3	1.5 ± 0.2	0.45 ± 0.2	1.5 ± 0.4	0.31 ± 0.3	-
E_g	-0.2 ± 0.08	0	-0.5 ± 0.2	0.02 ± 0.07	-1 ± 0.04	0
T_{2g}^2	0.13 ± 0.05	0.62 ± 0.05	0.3 ± 0.02	0.3 ± 0.02	0.44 ± 0.02	0.44 ± 0.02
A_{1g}	-0.4 ± 0.04	0.25 ± 0.03	-0.4 ± 0.03	0.14 ± 0.03	-1.2 ± 0.3	0
T_{2g}^4	-1.6 ± 0.3	1.1 ± 0.17	-0.7 ± 0.1	0.43 ± 0.1	-0.75 ± 0.2	0.87 ± 0.14

TABLE II. $\frac{d\Gamma}{dP}$ for various phonon modes below and above P_c

C. High-pressure Raman studies on SBIO ($x = 0.02$ and 0.10)

The pressure evolution of the Raman spectra of $x = 0.02$ and 0.10 are given in Figs. S2-S3, showing the same number of phonon modes up to the highest measured pressure. Figure 4 (a) and (d) shows fitted Raman spectra for SBIO ($x = 0.02$ and 0.10 , respectively) at a few representative pressures, marking E_g , A_{1g} , and three T_{2g} phonons. The corresponding phonon frequencies are presented in panels (b) and (e) of this figure, with pressure coefficients listed alongside the straight-line fits to the data. For all phonons, the frequency versus pressure plot fits with a single positive slope ($\frac{d\omega}{dP}$) over the whole recorded pressure range. The lack of slope change at P_c in doped $\text{Sm}_2\text{Ir}_2\text{O}_7$ can be understood by the fact that the IrO_6 octahedra are less deformed at ambient pressure due to a smaller value of the oxygen coordinate u , and the iso-structural rearrangement

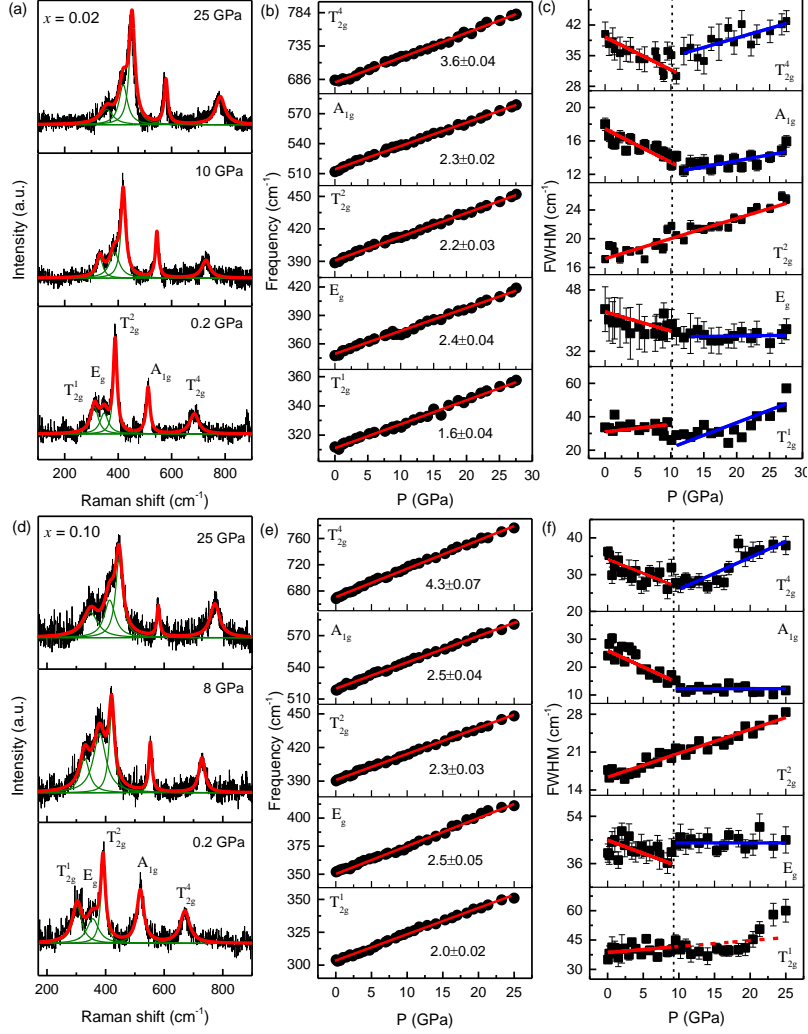


FIG. 4. (a,d) Fitted Raman spectra of SBIO ($x = 0.02$ and 0.10 , respectively) at some representative pressures. ((b,c) and (e,f) The pressure dependence of frequencies and linewidths of various phonon modes for $x = 0.02$ and 0.10 , respectively. Symbols and lines have the same meaning as Fig. 3.

is smaller as compared to the undoped sample. The linewidth of the A_{1g} , E_g , and T_{2g}^4 modes show anomalous decrease up to P_c (~ 10.2 and 9 GPa for $x = 0.02$ and 0.10 , respectively) as shown in panels (c) and (f) of Fig. 4, similar to the $x = 0$ sample. Figure 5 (a) depicts the evolution of the pressure coefficient of the linewidth ($\frac{d\Gamma}{dP}$) as a function of doping concentration (x) which demonstrates that the T_{2g}^4 phonon for $x = 0$ has a greater linewidth decrease than the A_{1g} and E_g phonons, whose amplitude decreases with Bi doping. The $\frac{d\Gamma}{dP}$ of the A_{1g} and E_g phonons is similar for $x = 0$ and 0.02 but increases significantly for $x = 0.10$ sample. These variations in the linewidths of A_{1g} , E_g , and T_{2g}^4 modes infer that the Ir-O-Ir bending and Ir-O

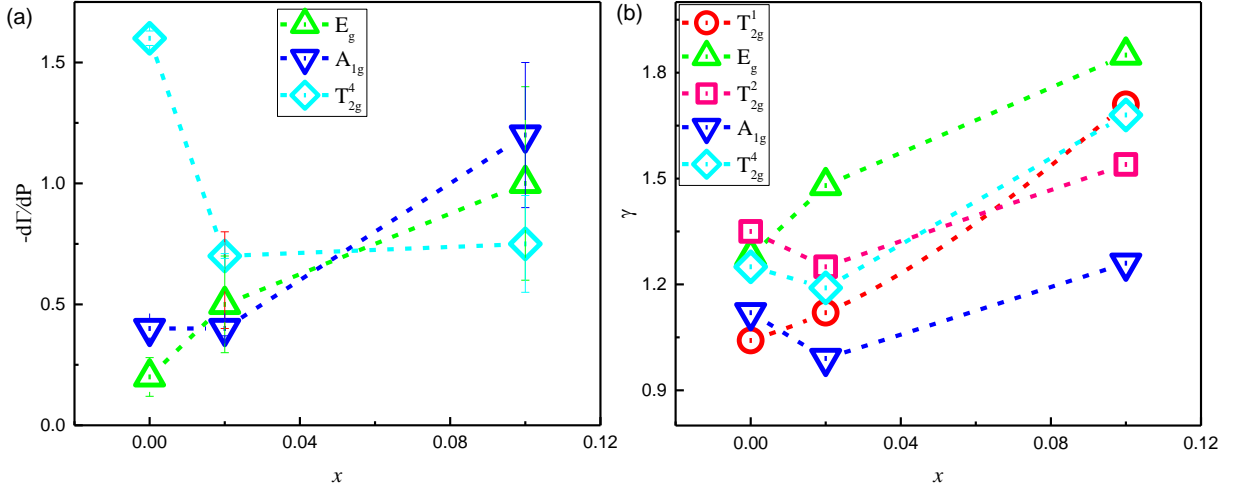


FIG. 5. (a,b) Evolution of $\frac{d\Gamma}{dP}$ and Grüneisen parameter below P_c (γ), respectively of various Raman phonons with doping concentration x . Dashed lines are guides to the eye.

bond stretching vibrations are influenced differently by electron-phonon interaction. Our Raman data clearly reveal that the crossover pressure P_c for the doped sample decreases gradually with x similar to $(\text{Eu}_{1-x}\text{Bi}_x)_2\text{Ir}_2\text{O}_7$ [25]. Figure 5 (b) shows the evolution of Grüneisen parameter (γ) (below P_c) with doping concentration x for five phonon modes, showing a monotonic increase, as in $(\text{Eu}_{1-x}\text{Bi}_x)_2\text{Ir}_2\text{O}_7$ [25], reflecting the increase of bulk modulus with x (see inset of Fig. 2 (c)).

IV. CONCLUSIONS

In summary, we have investigated pressure-induced structural changes in the $(\text{Sm}_{1-x}\text{Bi}_x)_2\text{Ir}_2\text{O}_7$ ($x = 0, 0.02, \text{ and } 0.10$) series using synchrotron-based X-ray diffraction and Raman-scattering measurements up to ~ 20 and 25 GPa, respectively. Our Raman and X-ray results suggest an isostructural phase transition associated with the rearrangement of IrO_6 octahedra in the pyrochlore lattice in $\text{Sm}_2\text{Ir}_2\text{O}_7$, at ~ 11.2 GPa. The transition pressure decreases to ~ 10.2 and 9 GPa for $x = 0.02$ and 0.10 , respectively due to an anomalous lattice contraction in SBIO series. The linewidths of the Ir-O-Ir bending (A_{1g} and E_g) and Ir-O stretching (T_{2g}^4) vibrations exhibit anomalous drop with increasing pressure up to P_c for all the samples, attributed to a decrease in electron-phonon interaction. The integration of Raman spectroscopy and XRD measurements in this study not only enhances the reliability of our observations but also allows for a comprehensive understanding of the structural changes occurring in SBIO under high pressure. Our findings contribute to the

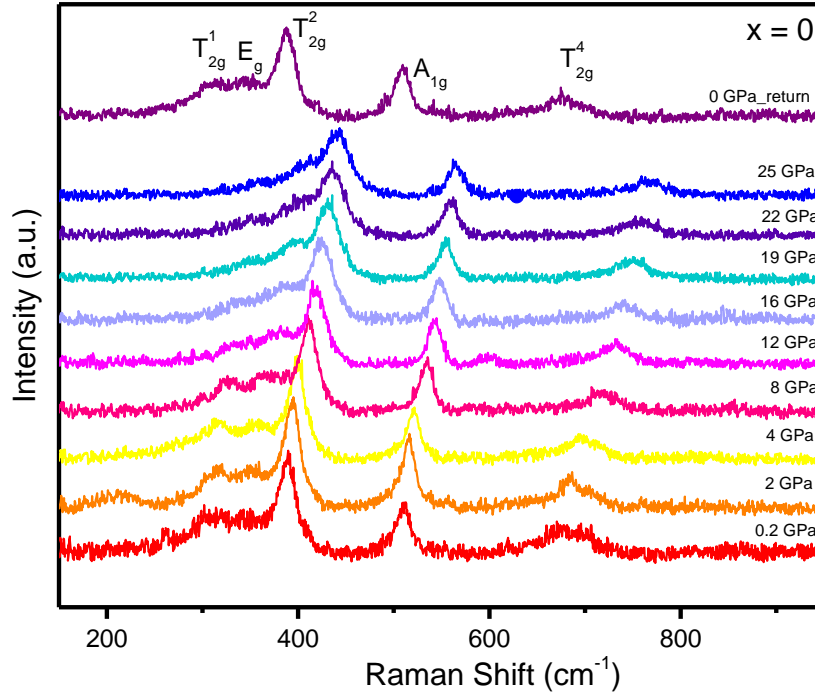


FIG. 6. [Fig.S1 : Pressure evolution of the Raman spectra for $x = 0$.]

fundamental understanding of pyrochlore iridates and hold potential implications for the design of materials with tailored properties and novel quantum states.

V. ACKNOWLEDGEMENT

AKS thanks the Department of Science and Technology, Government of India, for financial support under the National Science Chair Professorship. The authors acknowledge the financial support by the Department of Science and Technology (DST) of the Government of India for the high-pressure XRD measurements at the Xpress beamline of Elettra Sincrotrone, Trieste.

-
- [1] L. Savary, E.-G. Moon, and L. Balents, *Phys. Rev. X* **4**, 041027 (2014).
 - [2] X. Wan, A. M. Turner, A. Vishwanath, and S. Y. Savrasov, *Phys. Rev. B* **83**, 205101 (2011).
 - [3] W. Witczak-Krempa and Y. B. Kim, *Phys. Rev. B* **85**, 045124 (2012).
 - [4] K.-H. Ahn, K.-W. Lee, and W. E. Pickett, *Phys. Rev. B* **92**, 115149 (2015).
 - [5] M. Kargarian, J. Wen, and G. A. Fiete, *Phys. Rev. B* **83**, 165112 (2011).

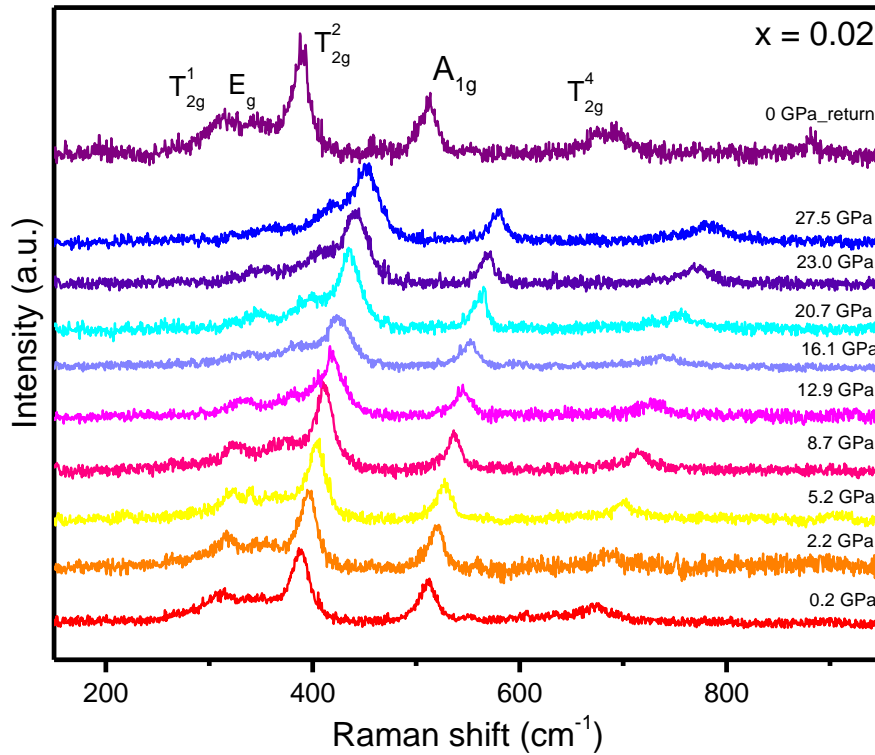


FIG. 7. [Fig.S2 : Pressure evolution of the Raman spectra for $x = 0.02$.]

- [6] S. M. Disseler, C. Dhital, A. Amato, S. R. Giblin, C. de la Cruz, S. D. Wilson, and M. J. Graf, *Phys. Rev. B* **86**, 014428 (2012).
- [7] C. Donnerer, M. C. Rahn, M. M. Sala, J. G. Vale, D. Pincini, J. Stempfer, M. Krisch, D. Prabhakaran, A. T. Boothroyd, and D. F. McMorrow, *Phys. Rev. Lett.* **117**, 037201 (2016).
- [8] M. Klicpera, K. Vlášková, and M. Diviš, *The Journal of Physical Chemistry C* **124**, 20367 (2020).
- [9] M. Graf, S. Disseler, C. Dhital, T. Hogan, M. Bojko, A. Amato, H. Luetkens, C. Baines, D. Margineda, S. Giblin, M. Jura, and S. Wilson, *Journal of Physics: Conference Series* **551**, 012020 (2014).
- [10] S. Nakatsuji, Y. Machida, Y. Maeno, T. Tayama, T. Sakakibara, J. v. Duijn, L. Balicas, J. N. Millican, R. T. Macaluso, and J. Y. Chan, *Phys. Rev. Lett.* **96**, 087204 (2006).
- [11] K. Matsuhira, M. Wakeshima, R. Nakanishi, T. Yamada, A. Nakamura, W. Kawano, S. Takagi, and Y. Hinatsu, *Journal of the Physical Society of Japan* **76**, 043706 (2007), <https://doi.org/10.1143/JPSJ.76.043706>.
- [12] H. Zhang, K. Haule, and D. Vanderbilt, *Phys. Rev. Lett.* **118**, 026404 (2017).
- [13] F. F. Tafti, J. J. Ishikawa, A. McCollam, S. Nakatsuji, and S. R. Julian, *Phys. Rev. B* **85**, 205104 (2012).

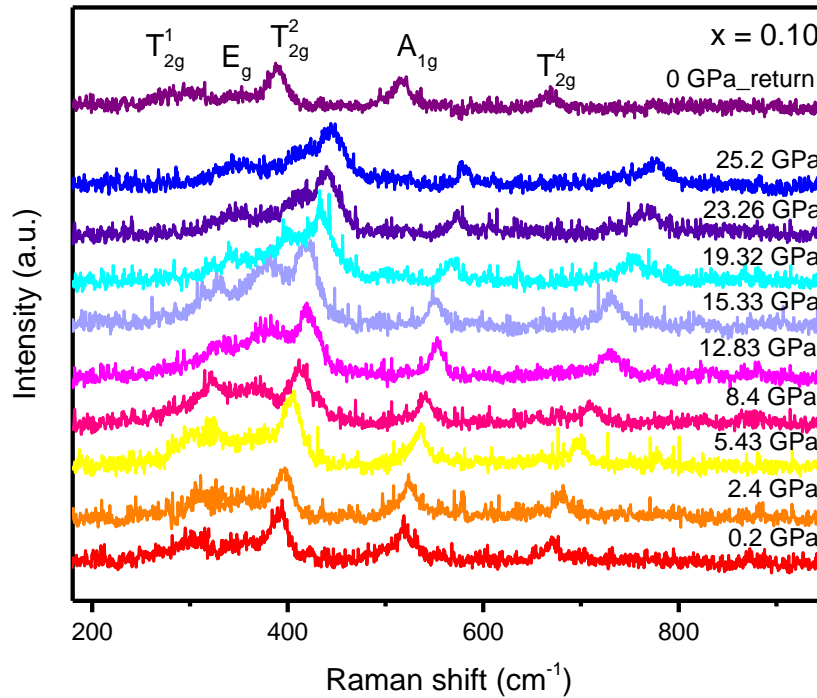


FIG. 8. [Fig.S3 : Pressure evolution of the Raman spectra for $x = 0.10$.]

- [14] P. Telang and S. Singh, (2021), [arXiv:2106.03512 \[cond-mat.str-el\]](https://arxiv.org/abs/2106.03512).
- [15] M. Rosalin, P. Telang, S. Singh, D. V. S. Muthu, and A. K. Sood, *Phys. Rev. B* **108**, 035133 (2023).
- [16] R. A. Forman, G. J. Piermarini, J. D. Barnett, and S. Block, *Science* **176**, 284 (1972), <https://www.science.org/doi/pdf/10.1126/science.176.4032.284>.
- [17] G. J. Piermarini, S. Block, J. D. Barnett, and R. A. Forman, *Journal of Applied Physics* **46**, 2774 (1975), https://pubs.aip.org/aip/jap/article-pdf/46/6/2774/18370506/2774_1_online.pdf.
- [18] A. Dewaele, P. Loubeyre, and M. Mezouar, *Phys. Rev. B* **70**, 094112 (2004).
- [19] A. P. Hammersley, *European Synchrotron Radiation Facility Internal Report ESRF97HA02T*. 68, pp. 58 (1997), [10.1103/PhysRevB.108.035133](https://arxiv.org/abs/10.1103/PhysRevB.108.035133).
- [20] A. Larson, R. Dreele, and B. Toby, Los Alamos Natl. Laboratory Report No. LAUR 86. **748** (4).
- [21] G. J. Piermarini, S. Block, and J. Barnett, *Journal of Applied Physics* **44**, 5377 (2003).
- [22] L. A. Deschenes, *Journal of the American Chemical Society* **122**, 9567 (2000).
- [23] F. Birch, *Journal of Geophysical Research: Solid Earth* **91**, 4949 (1986).
- [24] J. P. Clancy, H. Gretarsson, E. K. H. Lee, D. Tian, J. Kim, M. H. Upton, D. Casa, T. Gog, Z. Islam, B.-G. Jeon, K. H. Kim, S. Desgreniers, Y. B. Kim, S. J. Julian, and Y.-J. Kim, *Phys. Rev. B* **94**, 024408

(2016).

- [25] A. Thomas, P. Telang, D. Rout, K. Mishra, A. Pal, D. V. S. Muthu, P. S. A. Kumar, S. Singh, and A. K. Sood, *Pramana* **97**, 138 (2023).
- [26] D. Staško, K. Vlášková, A. Kancko, D. M. Többens, D. Daisenberger, G. Garbarino, R. H. Colman, and M. Klicpera, “Robustness of the pyrochlore structure in rare-earth $A_2Ir_2O_7$ iridates and pressure-induced structural transformation in IrO_2 ,” (2024), [arXiv:2403.00477 \[cond-mat.mtrl-sci\]](https://arxiv.org/abs/2403.00477).
- [27] P. Telang, K. Mishra, A. K. Sood, and S. Singh, *Phys. Rev. B* **97**, 235118 (2018).
- [28] M. Subramanian, G. Aravamudan, and G. Subba Rao, *Progress in Solid State Chemistry* **15**, 55 (1983).
- [29] S. Saha, D. V. S. Muthu, S. Singh, B. Dkhil, R. Suryanarayanan, G. Dhahlenne, H. K. Poswal, S. Karmakar, S. M. Sharma, A. Revcolevschi, and A. K. Sood, *Phys. Rev. B* **79**, 134112 (2009).
- [30] K. Ueda, R. Kaneko, A. Subedi, M. Minola, B. J. Kim, J. Fujioka, Y. Tokura, and B. Keimer, *Phys. Rev. B* **100**, 115157 (2019).
- [31] H. Kumar, V. G. Sathe, and A. K. Pramanik, *J. Phys. Chem. C* **127**, 13178 (2023).
- [32] S. Saha, D. V. S. Muthu, C. Pascanut, N. Dragoe, R. Suryanarayanan, G. Dhahlenne, A. Revcolevschi, S. Karmakar, S. M. Sharma, and A. K. Sood, *Phys. Rev. B* **74**, 064109 (2006).
- [33] H. Takatsu, K. Watanabe, K. Goto, and H. Kadowaki, *Phys. Rev. B* **90**, 235110 (2014).
- [34] A. Debernardi, C. Ulrich, M. Cardona, and K. Syassen, *physica status solidi (b)* **223**, 213 (2001).
- [35] P. M. Dee, J. Coulter, K. G. Kleiner, and S. Johnston, *Communications Physics* **3**, 145 (2020).
- [36] J. Serrano, A. Cantarero, M. Cardona, N. Garro, R. Lauck, R. E. Tallman, T. M. Ritter, and B. A. Weinstein, *Phys. Rev. B* **69**, 014301 (2004).